01 Jan 1993

Computed Versus Observed Inelastic Seismic Low-rise RC Shear Walls

Franklin Y. Cheng
Missouri University of Science and Technology, chengfy@mst.edu

G. E. Mertz

M. S. Sheu

J. F. Ger

Computed versus Observed Inelastic Seismic Low-Rise RC Shear Walls

By F. Y. Cheng,[1] Fellow, ASCE, G. E. Mertz,[2] M. S. Sheu,[3] and J. F. Ger,[4] Associate Member, ASCE

Abstract: A technique of calculating inelastic deformation of low-rise shear walls having height-width ratios of 0.5 and 0.75 without boundary elements is presented with consideration of the coupling effect for bending and shear deformations as well as the deformation due to base rotation. An interaction surface of moment, shear, and curvature or moment, shear, and shear strain is developed. The deflections at crack, yield, and ultimate loadings can be calculated separately from bending and shear deformations, which are compared favorably with experimental results. The shear deformation is significant for the low-rise walls studied because the deformation due to bending deformation is about 40–60% of the total deformation after the walls have reached 20% of ultimate deformation. The hysteresis rules are developed for both bending and shear deformations on the basis of theoretical and experimental studies. Favorable comparisons between the calculated and experimental responses were observed for individual walls and a low-rise two-story building on a shaking-table test. A computer program was developed for structural system analysis subjected to seismic excitations.

INTRODUCTION

Early experimental investigations on low-rise shear walls attempted to determine their strength to resist blast loadings from atomic weapons. These experimental investigations of reinforced concrete (RC) shear walls were performed by Galletly (1952), Benjamin and Williams (1957). The studies focused on the behavior of low-rise shear walls with boundary columns subjected to static monotonic loadings. Antebi et al. (1960) experimentally studied the behavior of low-rise shear walls with boundary elements subjected to dynamic blast loadings, and proposed an analytical method to calculate the dynamic strength of the walls. The studies by Galletly, Benjamin and Williams, and Antebi led to the development of design criteria for RC shear walls subject to blast loadings (Anderson et al. 1964).

Cardenas et al. (1980) studied walls with a height to width ratio of 1. In this study, boundary columns were not included, and the amount and distribution of reinforcement were the major variables studied. Results indicate that low-rise rectangular walls can develop shear stresses on the order of $10\sqrt{f_c'}$ psi.

Barda et al. (1976) tested low-rise shear walls with flanged boundary elements subject to both static monotonic and static cyclic loadings. The static cycling loadings were intended to represent the demands placed on the shear wall during a severe earthquake. The behavior of these walls was dominated by shear.

---

[1]Curators' Prof., Dept. of Civ. Engrg., Univ. of Missouri-Rolla, Rolla, MO 65401.
[2]Sr. Engr., Savannah River Tech. Ctr., Westinghouse Savannah River Co., Aiken, SC 29808.
[3]Prof., Dept. of Arch. Engrg., Nat. Cheng Kung Univ., Tainan, Taiwan.
[4]Postdoctoral Fellow, Dept. of Civ. Engrg., Univ. of Missouri-Rolla, Rolla, MO.
Note. Discussion open until April 1, 1994. To extend the closing date one month, a written request must be filed with the ASCE Manager of Journals. The manuscript for this paper was submitted for review and possible publication on July 31, 1992. This paper is part of the *Journal of Structural Engineering*, Vol. 119, No. 11, November, 1993. ©ASCE, ISSN 0733-9445/93/0011-3255/$1.00 + $.15 per page. Paper No. 4532.

Paulay et al. (1982) tested low-rise shear walls subjected to cycling loadings with and without boundary columns and having a height-to-width ratio of 0.54. One objective of the study was to determine methods to control sliding shear deformation. Paulay et al. (1982) proposed that the wall be designed such that the wall's shear capacity is greater than the flexural strength, thus forcing the wall to fail in flexure rather than shear.

Recent work in Japan by Watabe et al. (1989), among others, has focused on quantitative evaluation of load-deflection characteristics on heavily reinforced RC low-rise shear walls, normally used in nuclear-power-plant structures. The specimens have boundary columns, which are mainly subjected to monotonically increasing loading.

Research on squat RC shear walls in France has been carried out at the Centre Experimental de Recherches et d'Etudes du Batiment et des Travous Pulic. The primary objective is to determine the stiffness-degrading behavior of walls having different reinforcement ratios, varying from almost zero to 0.5%, in both horizontal and vertical directions. The results show that the stiffness is constant until cracking, and it declines severely after cracking. The stiffness begins to slowly decrease before the first diagonal shear crack appears (Coladant and Foure 1989).

The French Commissariat a l'Energie Atomique-Centre d'Etudes Nucleaires has studied the seismic behavior of RC low-rise shear walls (Wang et al. 1989). The results indicate that the dynamic behavior of shear walls depends strongly on the nonlinearity and the time history of the input force; the inelastic spectrum method underestimates the margin given by ductility for narrow-band excitation centered on the natural frequency of the wall. No experimental work was carried out, and the time-history analyses were performed by using the modified Takeda model, which has mainly bending deformation.

In the United States, work on RC low-rise shear wall has been undertaken at the Los Alamos National Laboratory (LANL). Dove et al. (1985) and Anderson et al. (1984) tested a series of small-scale shear walls and box-type structures subjected to both static and earthquake loadings. The purpose of these tests was to find the stiffness reduction and its effect on the natural frequency. They studied walls with height-to-width ratios varying from 0.25 to 1 and steel ratios from 0.25 to 0.6%. The tests showed a 75% stiffness reduction during a 0.75 g peak acceleration earthquake signal; the fundamental natural frequencies were reduced by factors of 2 or more over those calculated based on an uncracked cross section strength-of-materials approach.

From this literature review, one may observe that a great deal of research has been developed for low-rise shear walls. Most of the work, however, had specific goals of determining the ultimate capacity of the walls, stiffness reduction, or behavior under cyclic loading. The research results do not provide adequate information with which to develop hysteresis rules for isolated low-rise walls because: (1) Most of the walls subjected to either monotonic or cyclic loading had boundary elements; (2) the shear and bending deformations were not separated; and (3) the cyclic loading patterns used in the tests did not provide sufficient information with which to develop large- and small-amplitude loops for earthquake response studies. Low-rise buildings actually constitute a large percentage of total construction. Many of these buildings are braced by shear walls without boundary columns.

Therefore, it is necessary to perform experimental and analytical work to derive mathematical models for inelastic analysis. Under a joint research

project between the National Cheung Kung University (NCKU) in Taiwan and the University of Missouri-Rolla (UMR), Sheu (1988) at NCKU tested a series of isolated low-rise shear walls subjected to various static, monotonic, cyclic, and earthquake-type loadings. F. Y. Cheng and his associates at UMR have incorporated experimental data from NCKU and some from LANL to develop hysteresis rules and to investigate inelastic response behavior of individual walls and systems. This paper presents the method for calculating shear and bending deformations, and bending and shear hysteresis models considering large- and small-amplitude loops for the analysis of general low-rise shear wall structural systems. The analytical technique is based on Cheng's (1981) previous work and the results presented here are summarized from Cheng and Mertz (1989).

SELECTION OF SPECIMENS AND LOADING PATTERNS

The isolated low-rise shear walls tested at NCKU were rectangular in cross section. The walls have a width of 100 cm and a thickness of 10 cm, as shown in Fig. 1. The height varies from 50 cm to 75 cm, which gives height-to-width ratios from 0.50 to 0.75. The horizontal and vertical reinforcements consist of evenly spaced D10 through D19 bars, shown in Table 1 (and see Fig. 2); D10, D13, D16, and D19 are approximately equal to bar nos. 3, 4, 5, and 6, respectively. A 30-cm- × 30-cm-cap element is cast at the top of the wall, as shown in Fig. 1. Loads are applied at the centerline of this element. A 30-cm- × 55-cm-rigid base is cast at the base of the wall. This base is bolted to the test bed. Both the cap element and the rigid base are heavily reinforced.

The experimental displacements of the 50-cm-high walls were measured with the gages shown in Fig. 1. Gages 2, 3, 4, 5, 6, 7, 16, and 20 were used to measure vertical deformations. Gages 8 and 9 were used to measure the change in diagonal distance across the width of the wall. Gages 10, 11, 12, 13, 14, and 15 were used to measure the horizontal deformation of the wall. The experimental displacements of the 75-cm walls were measured with similar gages.

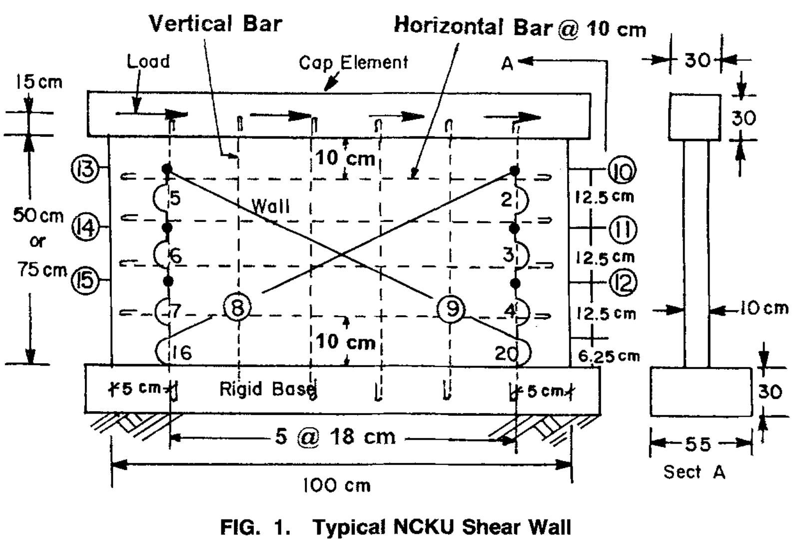

FIG. 1. Typical NCKU Shear Wall

TABLE 1. Test Specimens at NCKU

Wall (1)	$W \times H \times T$ (2)	f'_c (3)	Vertical Bars (4)	Vertical ρ (5)	Horizontal Bars (6)	Horizontal ρ (7)	f_y (8)	H/W (9)	Horizontal loading (10)
SW1a	100 × 50 × 10	275	6 D10	0.43	4 D10	0.57	4,930	0.50	cyclic[a]
SW3	100 × 50 × 10	278	6 D10	0.43	4 D10	0.57	4,930	0.50	earthquake[b]
SW4	100 × 50 × 10	270	6 D13	0.77	4 D13	1.03	4,900	0.50	monotonic[c]
SW4a	100 × 50 × 10	272	6 D13	0.77	4 D13	1.03	4,900	0.50	cyclic[a]
SW5	100 × 50 × 10	278	6 D13	0.77	4 D13	1.03	4,900	0.50	cyclic[d]
SW6	100 × 50 × 10	288	6 D13	0.77	4 D13	1.03	4,900	0.50	earthquake[b]
SW10	100 × 50 × 10	275	6 D13	0.76	4 D10	0.57	4,770	0.50	monotonic[c]
SW11	100 × 50 × 10	265	2 D19 3 D10	0.79	4 D10	0.57	4,770	0.50	cyclic[e]
SW12	100 × 50 × 10	270	2 D16 3 D13	0.78	4 D10	0.57	4,770	0.50	monotonic[c]
SW13	100 × 50 × 10	330	6 D13	0.76	none	0.00	4,770	0.50	monotonic[c]
SW14	100 × 50 × 10	320	6 D13	0.76	8 D10	1.14	4,770	0.50	monotonic[c]
SW15	100 × 75 × 10	265	2 D19 3 D10	0.79	6 D10	0.57	4,770	0.75	monotonic[c]
SW16	100 × 75 × 10	270	6 D13	0.76	6 D10	0.57	4,770	0.75	monotonic[c]
SW19	100 × 75 × 10	250	6 D13	0.76	none	0.00	4,770	0.75	monotonic[c]
SW20	100 × 75 × 10	210	6 D13	0.76	6 D10	0.57	4,770	0.75	monotonic[c]

[a]One-sided cyclic loading.
[b]Earthquake loading.
[c]Monotonic loading.
[d]Two-sided cyclic loading.
[e]Two-sided cyclic loading, with each cycle at a larger load level than the previous cycle.
Note: W = width; H = height; T = thickness; ρ = reinforcement ratio; f'_c = ultimate concrete stress; f_y = yielding steel stress; all units are in kg and cm.

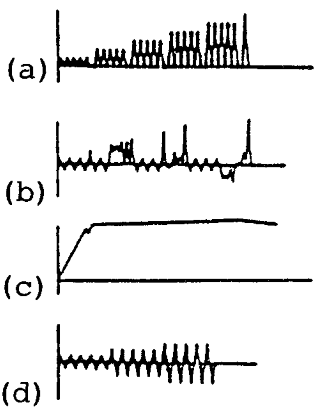

FIG. 2. Loading: (*a*) One-Sided Cyclic; (*b*) Earthquake; (*c*) Monotonic; (*d*) Two-Sided Cyclic

Four different loading patterns were used. There were one-sided cyclic loading, earthquake loading, monotonic loading, and two-sided-cyclic loading, as shown in Fig. 2. The adopted loading pattern for each wall is shown in Table 1.

ANALYSIS OF EXPERIMENTAL RESULTS

Bending and Shear Deformations

The curvature distributions for walls SW1a, SW3, SW4, SW4a, SW5, and SW6 were studied. The curvature can be calculated by taking the difference between longitudinal deformations at opposite sides of the wall and dividing by the horizontal distance of gages and the vertical length of the gage. For example, the curvature ϕ_1 is equal to $(\delta_5 - \delta_2)/(90 \times 12.5)$, where δ_2 and δ_5 are the longitudinal deformations at gages 2 and 5, respectively. Similarly, curvatures ϕ_2, ϕ_3, and ϕ_4 are equal to $(\delta_6 - \delta_3)/(90 \times 12.5)$, $(\delta_7 - \delta_4)/(90 \times 12.5)$, and $(\delta_{16} - \delta_{20})/(90 \times 6.25)$, respectively.

The experimentally observed crack pattern on the face of wall SW1a is shown in Fig. 3(*a*). This crack pattern corresponds to a point near the wall's ultimate load. The load and cycle at which the crack was first observed are represented in Fig. 3 by the "load(cycle number)," in which the load is in tons and cycle numbers are in the loading diagram shown in Fig. 3(*b*). As the wall is loaded a flexural crack opens up at the base of the wall, labeled "A" in Fig. 3(*a*); a diagonal shear crack forms, labeled "B;" and a flexural crack also forms in the wall at 12 tons during cycle 6, as shown by curve "C."

Wall SW1a has diagonal shear cracks under gage 5. As these cracks form they have a vertical component of deformation. The deformation of gage 5 is used to calculate the curvature ϕ_1, of which the experimentally measured values are influenced by shear deformation. Since: (1) The moment and shear are strongly coupled; (2) the curvature is influenced by the diagonal shear crack; and (3) the curvature is very sensitive to the crack location, then an average curvature is used to calculate the bending deformations. Thus the average curvature in the 50-cm walls is

$$\phi_{ave} = \frac{(\phi_1 + \phi_2 + \phi_3 + \phi_4)}{4} \quad (1)$$

and the bending deformation (or displacement) is

$$D_b = \frac{(43.75)^2}{2} \phi_{ave} \quad (2)$$

The shear deformation is then determined by subtracting the bending deformation from the total deformation

$$D_s = D_t - D_b \quad (3)$$

where D_t = total deformation, which can be calculated as

$$D_t = \frac{\delta_{13} + \delta_{10}}{2} \quad (4)$$

It is worthwhile mentioning that if diagonal gages 8 and 9 are used to calculate shear deformation, they will misinterpret a portion of the bending deformation due to flexural crack and label it as shear deformation. This was also recognized by Ma et al. (1976).

Fig. 4 indicates the ratio of bending deformation to total deformation for 50-cm-high walls. It shows that after deformation of 20% of the ultimate deformation, the bending deformation ranges between 40% and 60% of the total deformation for most walls. Wall SW11 has very large shear deformations before failure and the bending deformation only accounts for 10%

J. Struct. Eng., 1993, 119(11): 3255-3275

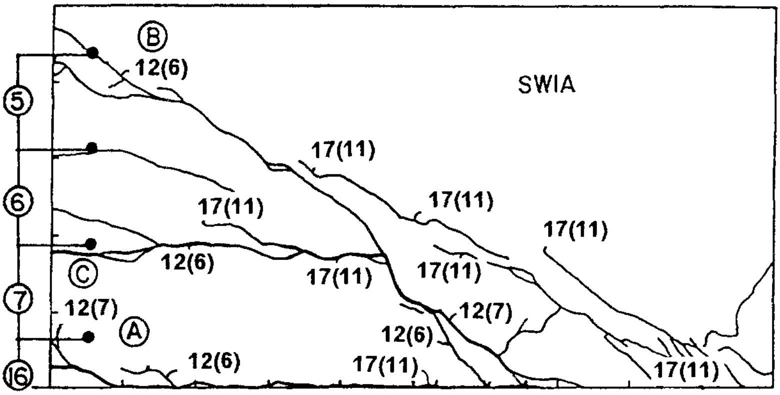

(a)

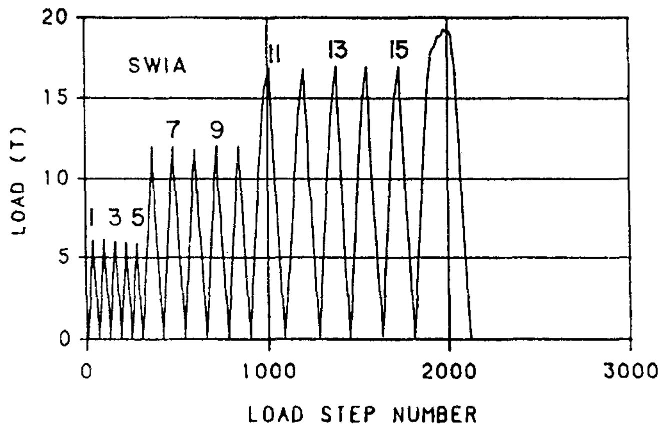

(b)

FIG. 3. NCKU SW1a Wall: (*a*) Surface Cracks; (*b*) Loading History

of the total deformation at failure. This wall is different from other walls because it has concentrated steel near the vertical edges. Bending deformation in the 75-cm walls has a percentage of total deformation that is similar to that in the 50-cm walls.

Note that the transverse reinforcing steel is omitted on walls SW13 and SW19 (see Table 1). If the traditional concept that transverse reinforcing steel resists shear and longitudinal reinforcing steel only resists bending were true, then the shear deformation for two walls should be larger than the walls with transverse reinforcing steel. However, the percentages of bending deformation in walls SW13 and SW19 are similar to those for the other walls.

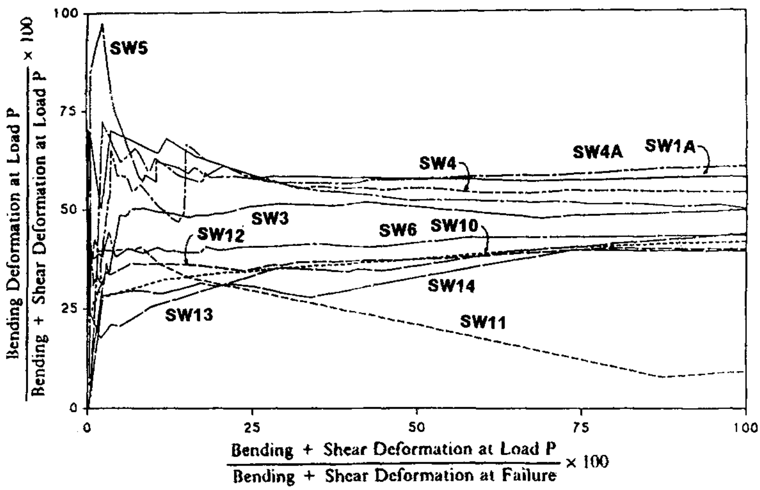

FIG. 4. Ratio of Bending Deformation to Total Deformation

Failure Ductility and Excursion Ratio

The displacement definition of ductility and excursion ratio for six of the shear walls is calculated. The ductility is given by

$$\mu_b = \frac{|D_{b_{ult}}|}{D_{b_y}} \qquad (5a)$$

$$\mu_s = \frac{|D_{s_{ult}}|}{D_{s_y}} \qquad (5b)$$

where $D_{b_{ult}}$ and $D_{s_{ult}}$ = bending and shear deformations at the ultimate load; and D_{b_y} and D_{s_y} = bending and shear deformations at yield load. The yield load corresponds to an average strain of $\varepsilon_y = 0.0024$ in the longitudinal steel reinforcing bar. The excursion ratio is given by

$$e_b = \sum (\mu_b - 1) \qquad (6a)$$

$$e_s = \sum (\mu_s - 1) \qquad (6b)$$

where the summation is carried out for each half-load cycle. The bending and shear failure ductilities and failure excursion ratios of walls SW1a, SW3, SW4, SW4a, SW5, and SW6 are calculated; the average bending failure ductility is 10.39 and the average shear failure ductility is 11.00. There is no significant pattern of failure ductility for any given loading history or wall-reinforcement ratio. Thus a ductility of 10 is set as the failure limit for both bending and shear ductilities. However, the walls with an earthquake loading (SW3 and SW6) have excursion ratios that are significantly larger than the other walls.

Ratios of Horizontal to Vertical Expansion

The average vertical strain of the 50-cm-high walls is determined by

$$\varepsilon_v = \frac{\delta_2 + \delta_3 + \delta_4 + \delta_{20} + \delta_5 + \delta_6 + \delta_7 + \delta_{16}}{2 \times 43.75} \qquad (7)$$

and the average horizontal strain is given by

$$\varepsilon_h = \frac{\delta_{10} + \delta_{11} + \delta_{12} + \delta_{13} + \delta_{14} + \delta_{15}}{3 \times 100} \quad \text{(8)}$$

where positive strain indicates expansion. The horizontal strain is plotted against the vertical strain in Fig. 5 for walls SW1a, SW3, SW4, SW4a, SW5, and SW6. The vertical strain is typically 2 to 8 times larger than the horizontal strain because the vertical expansion is not restrained except by the weight of the wall. The horizontal expansion is restrained by the heavily reinforced horizontal elements at the top and bottom of the wall and by the reinforcing steel.

MATHEMATICAL MODELING OF BACKBONE CURVES

Stress and Strain in Concrete and Steel

For a given wall configuration there exists a unique relationship between moment (M), shear (V), curvature (ϕ), and shear strain (γ), expressed as M-V-ϕ-γ. Let the bending strain be linear with respect to the width of the wall; the strain distribution is then determined by the tensile strain (ε_1) and compressive strain (ε_2) at the edges of the wall. Curvature ϕ is the slope of the linear strain distribution. Shear strain γ is assumed to be constant across the width of the wall. Because the horizontal expansion of the wall is restrained by the elements at the top and bottom of the wall, the horizontal expansion is much less than the vertical expansion (Fig. 5). Thus the transverse strain is consequently assumed to be zero. The combined bending and shear strain of any point in a wall is represented in Fig. 6.

Since both normal and shear strains act on a concrete element, Mohr's circle is used to determine the principal concrete compressive strain ε_{pc}, the

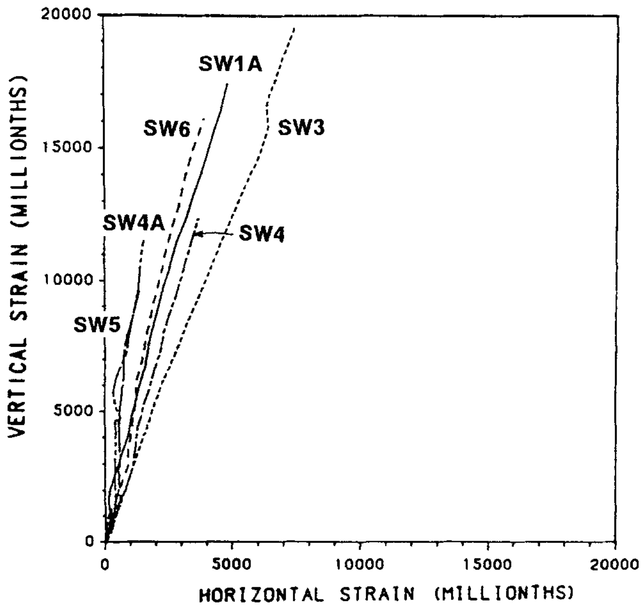

FIG. 5. Vertical versus Horizontal Expansion of NCKU Shear Walls

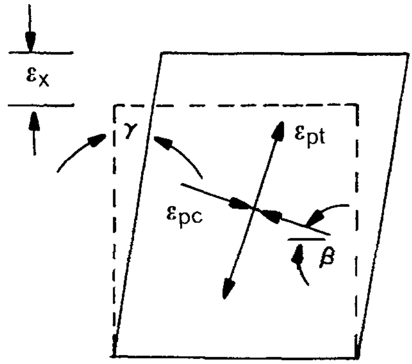

FIG. 6. Combined Bending and Shear Strains at Any Point in Shear Walls

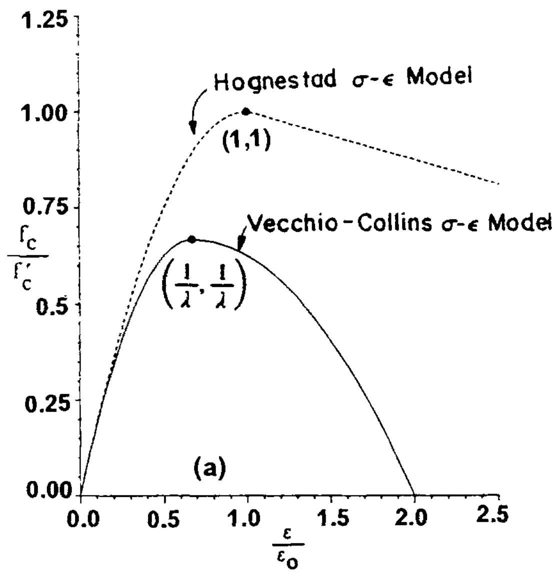

FIG. 7. Concrete Principal Compressive Stress-Strain Models

principal concrete tensile strain ε_{pt}, and the angle of orientation β. The principal concrete compressive stress σ_{pc} is softened to account for tensile strain that exists perpendicular to the principal compressive strain. The softening term $1/\lambda$ in the Vecchio-Collins stress-strain model (Vecchio and Collins 1982) controls the amount of softening as given in Fig. 7, in which f'_c = ultimate concrete compressive stress; f_c = concrete compressive stress; ε_0 = concrete strain at f'_c; and ε = concrete compressive strain; Hognestad's stress-strain model was given for concrete subject to uniaxial compression. Since a biaxial state of stress exists in a shear wall, Hognestad's model cannot be used without modification (Hsu and Mo 1984). The Vecchio-Collins stress-strain model is used for the present study. The concrete tensile stress-strain has had several models for it (Gilbert and Warner 1978), such as the gradual unloading model, the stepped stress-strain model, and the

J. Struct. Eng., 1993, 119(11): 3255-3275

discontinuous unloading model. Each of these models has at least one discontinuity when concrete cracks. A discontinuous tensile stress-strain model will cause the shear and bending backbone curves to be discontinuous; whereas the cracking in a shear wall is observed to be a more gradual process. Here, the gradual tensile stress-strain model is developed to provide a smooth transition between cracked and uncracked concrete. The graded tensile model for determining the principal tensile stress (σ_{pt}) used for the study is defined as

$$\text{if } \eta \leq 0.25 \quad \text{then} \quad \sigma_{pt} = E_c \varepsilon_{pt} \qquad (9a)$$

$$\text{if } 0.25 \leq \eta \leq 0.50 \quad \text{then} \quad \sigma_{pt} = f'_{cr}\,(0.0631 + 0.7476\eta) \qquad (9b)$$

$$\text{if } 0.50 \leq \eta \leq 0.75 \quad \text{then} \quad \sigma_{pt} = f'_{cr}\,(0.1907 + 0.4924\eta) \qquad (9c)$$

$$\text{if } 0.75 \leq \eta \leq 1.00 \quad \text{then} \quad \sigma_{pt} = f'_{cr}\,(0.3845 + 0.2340\eta) \qquad (9d)$$

$$\text{if } 1.00 \leq \eta \leq 25 \quad \text{then} \quad \sigma_{pt} = f'_{cr}\,(0.6443 - 0.0258\eta) \qquad (9e)$$

$$\text{if } 25 \leq \eta \quad \text{then} \quad \sigma_{pt} = 0 \qquad (9f)$$

and

$$\varepsilon_{cr} = \frac{f'_{cr}}{E_c} \qquad (10a)$$

and

$$\eta = \frac{\varepsilon_{pt}}{\varepsilon_{cr}} \qquad (10b)$$

where f'_{cr} = concrete tensile crack stress; ε_{cr} = concrete strain at f'_{cr}; and E_c = modulus of elasticity for concrete. This model provides a smooth transition between uncracked and cracked concrete in order to generate continuous M-V-ϕ-γ relationships. The concrete principal compressive and tensile stresses have the same orientation as their respective principal strains. Mohr's circle for stresses is used to determine the longitudinal concrete stress σ_{cl} and shear stress τ_c. The experimentally measured steel stress-strain curves for the steel bars in NCKU walls are used for the present study.

Interaction Surfaces

Given a longitudinal strain distribution ε_1 and ε_2 and a shear strain γ, the axial load, moment, and shear are determined by integrating stresses numerically over the wall's cross section. Typically, the maximum longitudinal compressive strain ε_2 is fixed and the maximum longitudinal tensile strain ε_1 is varied until the sum of axial loads is approximately zero. Several iterations are usually required before a strain distribution is acceptable. Repeating these calculations for different combinations of ε_2 and γ defines the moment-shear-curvature (M-V-ϕ) interaction surface [Fig. 8(*a*)] and the moment-shear-shear strain (M-V-γ) interaction surface [Fig. 8(*a*)].

Backbone Curves for Bending and Shear

At the base of the shear wall, the longitudinal steel reinforcing bars have a very high tensile stress. A slip is then developed in the bars. This deformation allows the wall to rotate as a rigid body about its base, causing additional lateral deformation at the top of the wall (Vallenas et al. 1979; Cheng and Mertz 1989). By calculating the base rotation θ_{br} for each point

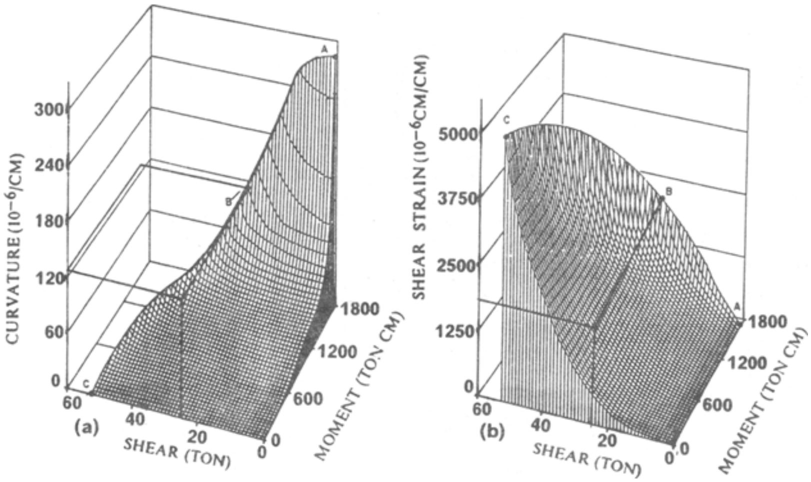

FIG. 8. Interaction Surfaces: (a) M-V-ϕ; **(b)**M-V-γ

on the M-V-ϕ interaction surface, an M-V-ϕ_{br} interaction surface can be obtained (Cheng and Mertz 1989). The deformation of a shear wall due to base rotation D_{br} is given by

$$D_{br} = \theta_{br} h \quad (11)$$

where θ_{br} = base rotation; and h = height of the wall.

Since the average curvature is assumed for the entire wall as shown in (1), the corresponding moment on the wall is constant. Treating the curvature distribution as a conjugate beam, the bending deformation (including base rotation of a low-rise shear wall for a given moment-to-shear ratio) is given by

$$D_b = \left(\frac{\theta_{br}}{h} + \frac{\phi}{2}\right) h^2 = \theta_u h^2 \quad (12)$$

where θ_u = bending rotation of a unit length wall. The shear strain (γ) is then determined from the M-V-γ interaction surface. Thus the shear deformation (D_s) is given by

$$D_s = \gamma h \quad (13)$$

The bending displacement (D_b), shear displacement (D_s), and total displacement ($D_t = D_b + D_s$) versus applied load for walls SW5 and SW6 are given in Fig. 9. The loads are applied at a point 65 cm above the base of the walls as shown in Fig. 1. Overall, the comparison between the calculated and experimental results for these walls is good. However, the calculated response typically slightly underestimates the lateral load at failure.

BENDING AND SHEAR HYSTERESIS MODELS

The hysteresis models for bending and shear deformations are developed based on the experimental data from NCKU shear walls SW1a, SW3, SW4a, SW5, and SW6. The models are sketched in Figs. 10 and 11, from which several rules are briefly summarized as follows.

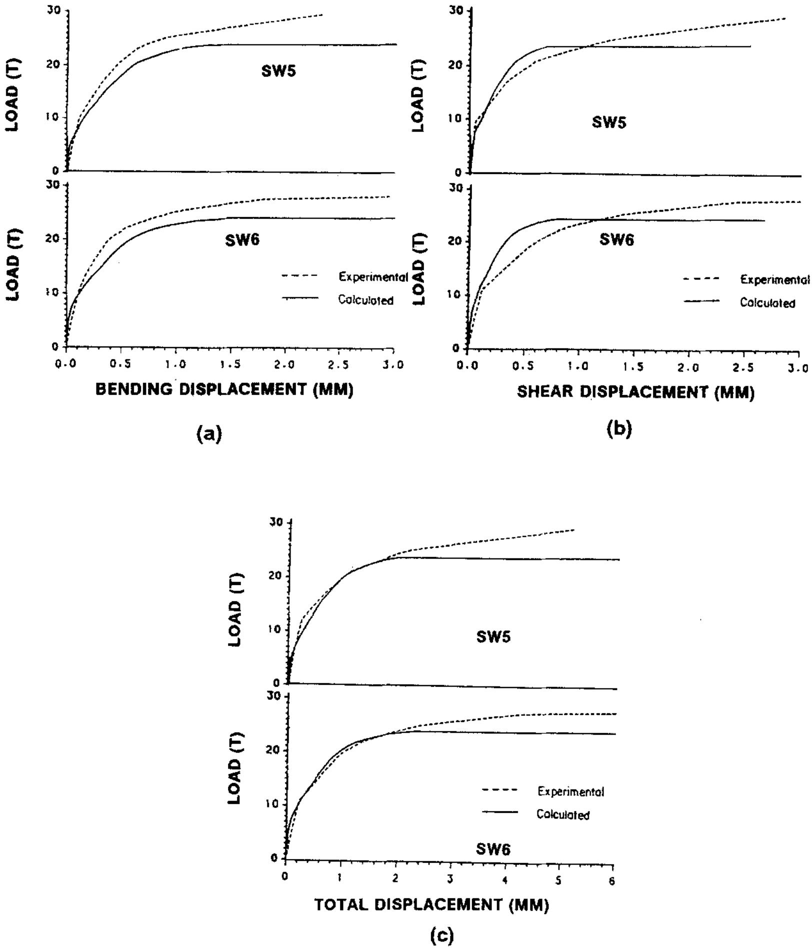

FIG. 9. Calculated and Experimental Monotonic Responses: (*a*) Bending Displacements; (*b*) Shear Displacements; and (*c*) Total Displacements

Loading on Backbone Curve

Backbone curves are defined in terms of applied load P and bending deformation D_b or shear deformation D_s. These backbone curves are linear up to the cracking load Pc, as shown in Figs. 10 and 11. Beyond the cracking point, the stiffness gradually decreases as successive reinforcing bars yield.

Unloading from Backbone Curve

The experimentally observed unloading curves are nonlinear, with a high initial stiffness that decreases with the load level. Semiempirical models are used for both the bending and shear unloading curves. Both the bending and shear unloading curves are represented by three linear segments. However, since different mechanisms influence the bending and shear deformations, the unloading stiffnesses are different.

The bending hysteresis model unloads from the maximum past load and

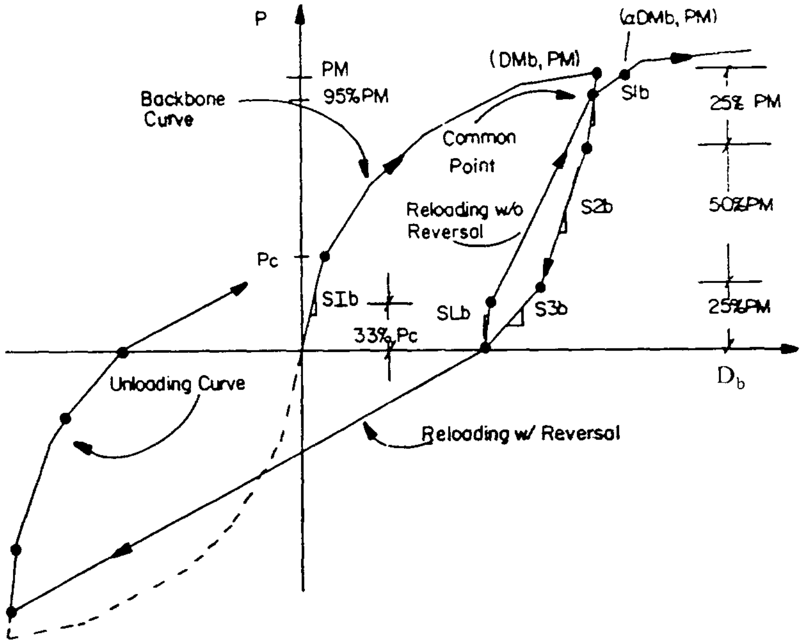

FIG. 10. Bending Hysteresis Model

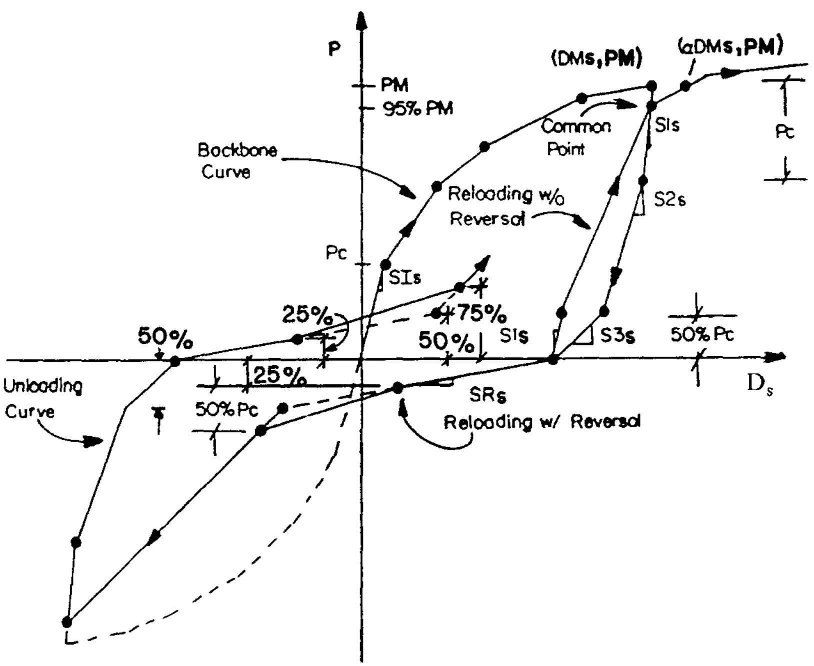

FIG. 11. Shear Hysteresis Model

J. Struct. Eng., 1993, 119(11): 3255-3275

displacement (PM, DMb) with a stiffness of $S1b$ for 25% PM (Fig. 10), with a stiffness of $S2b$ for 50% PM, and with a stiffness of $S3b$ for the remaining 25% PM; $S1b$, $S2b$, and $S3b$ are given by

$$S1b = SIb\left(\frac{Dcb}{Dbmax}\right)^{0.294} \quad \text{(14a)}$$

$$S2b = SIb\left(\frac{0.8344Dcb}{Dbmax} + 0.1656\right) \quad \text{(14b)}$$

$$S3b = SIb\left(\frac{0.9092Dcb}{Dbmax} + 0.0908\right) \quad \text{(14c)}$$

where SIb = initial bending precracking stiffness; Dcb = bending cracking displacement; and $Dbmax$ = absolute value of the maximum bending displacement in either direction.

The shear hysteresis model unloads from the maximum past load and displacement (PM, DMs), with a stiffness of $S1s$ for Pc (Fig. 11), with a stiffness of $S2s$ to a load of 50% Pc, and with a stiffness of $S3s$ for the remaining load; $S1s$, $S2s$, and $S3s$ are given by

$$S1s = 1.4675SIs\left(\frac{Dcs}{Dsmax}\right)^{0.343} \leq SIs \quad \text{(15a)}$$

$$S2s = 0.7761SIs\left(\frac{Dcs}{Dsmax}\right)^{0.32} \quad \text{(15b)}$$

$$S3s = SIs\left(\frac{1.369Dcs}{Dsmax} + 0.0707\right) \leq SIs \quad \text{(15c)}$$

where SIs = initial shear precracking stiffness; Dcs = shear cracking displacement; and $Dsmax$ = maximum shear displacement in either direction.

Reloading without Load Reversal

Both the bending and shear hysteresis models represent reloading with a bilinear curve. The stiffness of the first bending curve is

$$SLb = SIb\left(\frac{Dcb}{Dbmax}\right)^{0.285} \quad \text{(16)}$$

which acts over a load range of 33% Pc (Fig. 10). The second segment loads to a point common to both the unloading and loading curves, at 95% PM. The shear model is similar to the bending model except the stiffness of the first shear curve is $S1s$, which acts over a load range of 50% Pc (Fig. 11). The common point of the shear model is also at 95% PM.

Reloading above Common Point

When the wall is cycled at a constant load level, the displacements tend to increase from one load cycle to another. Both models reload above the common point, with a transition curve that passes from the common point, through (αDMb, PM) or (αDMs, PM), to the backbone curve (Figs. 10 and 11). For bending hysteresis model, α = 1.129 for the first cycle at a

J. Struct. Eng., 1993, 119(11): 3255-3275

given load; and $\alpha = 1.029$ for subsequent cycles at the same load. For the shear hysteresis model, $\alpha = 1.04$ for any cycle.

Reloading with Load Reversal

Large stable hysteresis loops were observed in bending test data. Thus, the bending hysteresis model reloads toward a fictitious common point, in the new loading direction. This common point is also at 95% *PM*, on a fictitious unloading curve.

The behavior of the shear hysteresis loop upon reloading is dominated by pinching. The pinching behavior is represented by three linear segments. The first segment has a stiffness of

$$SRs = SIs\left(\frac{Dcs}{Dsmax}\right)^{1.02} \quad \text{(17)}$$

and loads to 50% *Pc* (Fig. 11). The third segment loads from terminal end of the first, to a fictitious common point in the new direction. The second segment is a transition curve that joints the first and third segments from 25% *Pc* to 75% *Pc* and acts over a load range of 50% *Pc*.

Small Amplitude Hysteresis Loops

When the wall is cycled below the common point, small-amplitude hysteresis loops are formed. These loops have a stable shape. For unloading inside a small amplitude loop, both models unload parallel to the unloading curves just discussed. For loading inside small-amplitude loops, both the bending and shear models load toward last point where unloading began. However, the shear hysteresis model maintains pinched loops (Cheng and Mertz 1989).

Comparison between Hysteresis Models and Experimental Results

NCKU wall SW6 was subjected to a quasi-static earthquake loading. The experimental and analytical responses for the bending deformation are sketched in Fig. 12; the responses for shear deformation are presented in Fig. 13. Comparing the calculated and experimental responses, we note: (1) The unloading branches of both the shear and bending hysteresis models are well represented; (2) the reloading without load-reversal branches is also well represented; (3) the common point of 95% *PM* is reasonable; (4) the increase in displacements between loading cycles is similar; (5) the pinching behavior of the shear hysteresis model is reasonable; (6) the small-amplitude loops are accurate; and (7) both calculated and experimental responses dissipate similar amounts of energy (Cheng and Mertz 1989). Similar results for other walls are observed. Overall, these examples illustrate the accuracy of the bending and shear hysteresis models, and their applicability to complex loading histories.

SHEAR WALL ELEMENT STIFFNESS MATRIX

To study the response behavior of three-dimensional structural systems, a shear wall element was developed that utilizes the bending and shear hysteresis models. The shear wall element consists of a panel linking four joints (Fig. 14). Nonlinear bending and shear deformations in the plane of the wall are considered, along with nonlinear axial deformation. The bending, shear, and axial deformations are lumped into three nonlinear springs.

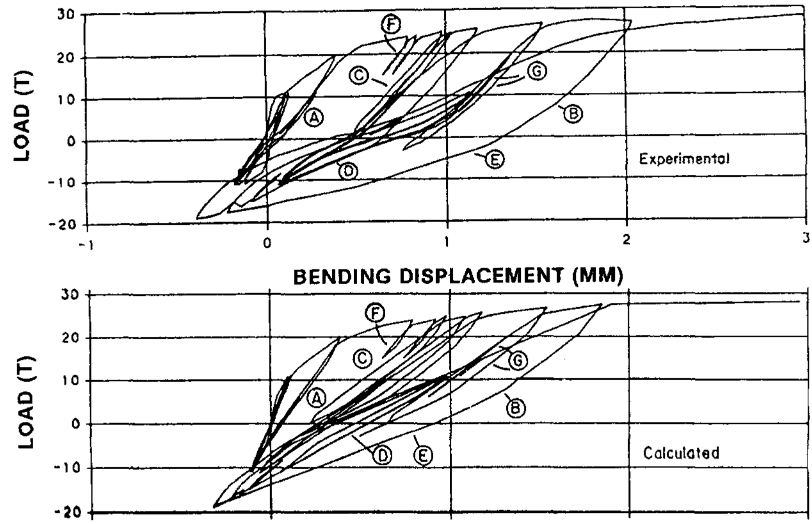

FIG. 12. Comparison of Calculated and Experimental Bending Hysteresis Loops for NCKU Wall SW6

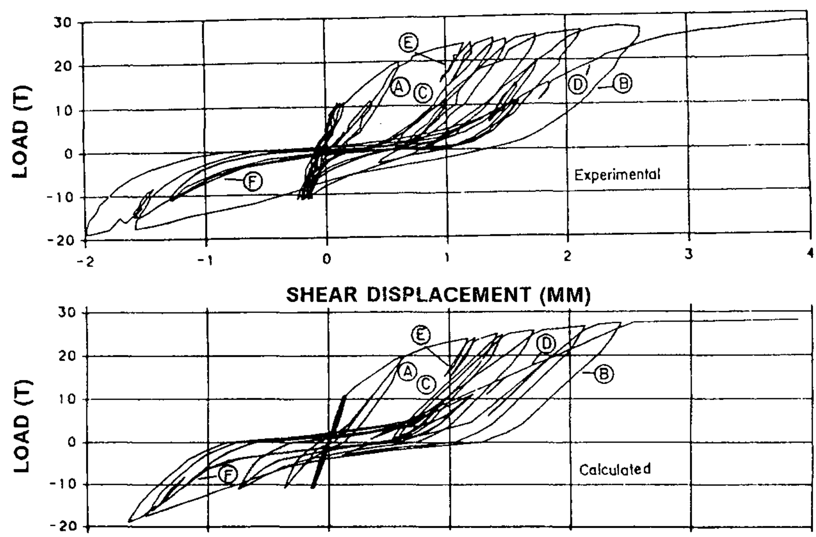

FIG. 13. Comparison of Calculated and Experimental Shear Hysteresis Loops for NCKU Wall SW6

A rigid body connects the joints at the top of the wall with the springs, while a second rigid body connects the joints at the bottom of the wall with the springs.

Let K_b, K_s, and K_a represent, respectively, the bending, shear, and axial stiffness of a unit height wall. The bending backbone curve and hysteresis model just mentioned can be expressed in terms of moment and unit height rotation as

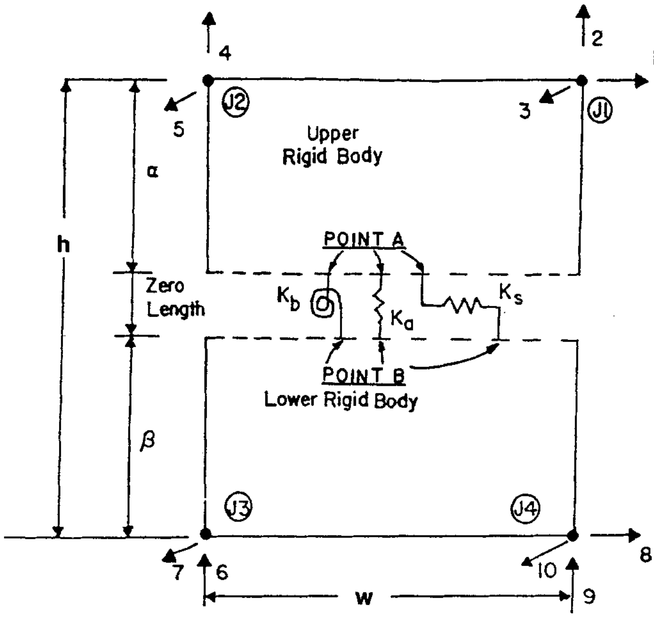

FIG. 14. Shear Wall Element

$$M = K_b\theta_u \qquad (18)$$

in which $M = P \times h$; and θ_u can be obtained from (12). Similarly, the shear backbone curve and hysteresis model can be expressed in terms of shear and shear strain as

$$V = K_s\gamma \qquad (19)$$

in which $V = P$; and γ can be obtained from (13). The axial hysteresis model adopted here was developed by Kabeyasawa et al. (1983) for shear walls. The shear wall's stiffness is given by

$$[K_e] = [A_2][A_1][SI]([A_2][A_1])^T \qquad (20)$$

where [SI] = spring stiffness matrix

$$[SI] = \frac{1}{h}\begin{bmatrix} K_b & 0 & 0 \\ 0 & K_s & 0 \\ 0 & 0 & K_a \end{bmatrix} \qquad (21)$$

$[A_1]$ = transformation matrix transferring three spring forces to points A and B on the edge of upper and lower rigid bodies, as shown in Fig. 14; and $[A_2]$ = transformation matrix that transfers forces from points A and B to the degrees of freedom at four joints. The element has 10 translational degrees of freedom. Degrees of freedom 2, 4, 6, and 9 represent axial deformation and bending rotations; and degrees of freedom 3, 5, 7, and 10 represent the out-of-plane geometric stiffness (Cheng 1993). Degrees of freedom 1 and 8 are used to represent in-plane shear and bending deformations.

A two-story auxiliary box structure called LANL 3D-11 was dynamically tested on a uniaxial shaking table by Dove et al. (1985) of the Los Alamos National Laboratory. The structural model is shown in Fig. 15. The direction of motion coincides with the structure's global Y-axis. The structural model consists of eight shear wall elements. The mass center and rigidity center of the structure coincide. The second floor and roof slabs are assumed to be rigid diaphragms. The input ground motion for dynamic analysis is a scaled version of the 1940 El Centro N-S earthquake (Dove et al. 1985). Damping is assumed to be 5%. The dynamic equation is solved by the method used previously by Cheng (1981), with time step of $\Delta t = 0.00001$ sec.

The calculated and experimental displacements for the roof are compared in Fig. 16(a). Overall, the comparison between calculated and experimental displacements is good. The calculated period is close to the experimental period. Both calculated and experimental results yield a similar frequency spectrum, as shown in Fig. 16(b). A strong 83-Hz acceleration signal is observed in both spectra, at which the calculated acceleration is close to the experimental acceleration. Between 200 and 300 Hz, the calculated response is larger than the experimental response.

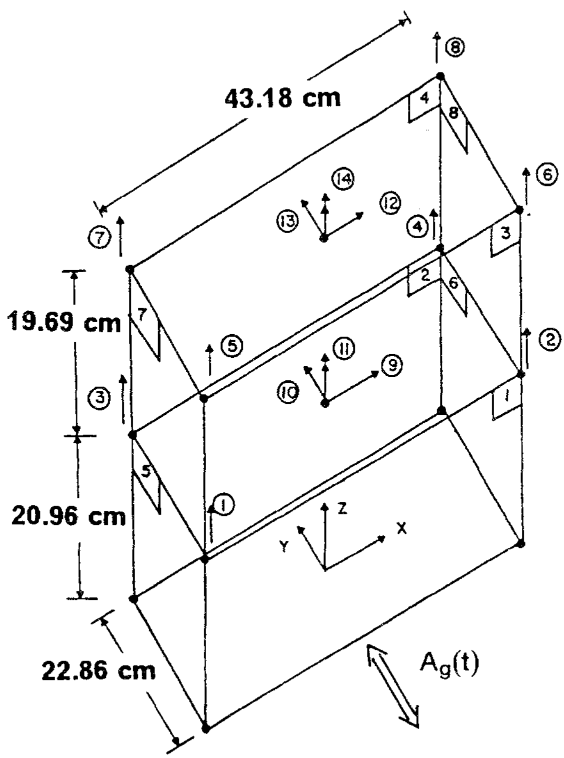

FIG. 15. LANL Two-Story Box-Type Structure

J. Struct. Eng., 1993, 119(11): 3255-3275

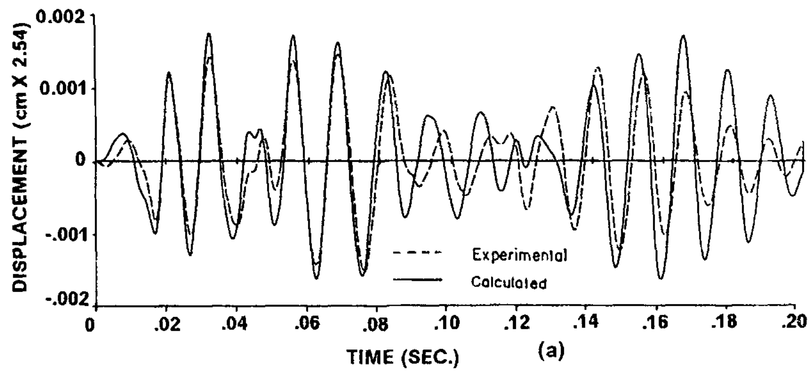

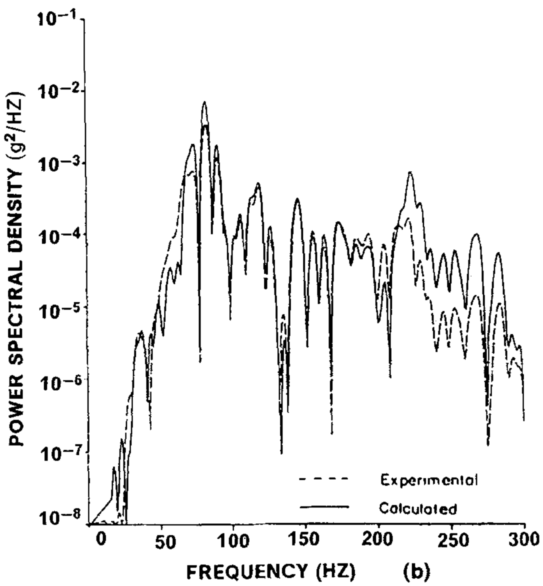

FIG. 16. Comparison of Calculated and Experimental Results: (*a*) For Roof Displacement; (*b*) For Power Spectrum Density

CONCLUSIONS

Shear and bending backbone curves and shear and bending hysteresis models of low-rise reinforced concrete shear walls without boundary elements were presented. The backbone curves and the hysteresis models were developed based on coupling behavior of bending and shear. Comparisons between the analytical and experimental results of walls with various steel ratios and loading types for backbone curves and hysteresis models are good. The formulation of the shear wall stiffness element based on hysteresis models was derived and used for analysis of three-dimensional structural systems. An excellent comparison between the calculated and the experi-

J. Struct. Eng., 1993, 119(11): 3255-3275

mental response on a shaking table test was also observed. The method presented can be used for: (1) Separation of shear and bending deformation from a total displacement at various loading stages of crack, yield, and ultimate; (2) elastic and inelastic analysis of low-rise shear-wall buildings subjected to static load and seismic excitations; and (3) evaluation of ductilities due to shear and bending for design specifications. For the low-rise walls studied, the shear deformation becomes more significant after elastic loading; the deflection due to bending deformation is about 40–60% of the total after the walls have reached 20% of ultimate deformation. Horizontal reinforced bars have little effect on the shear deformation of low-rise walls.

ACKNOWLEDGMENTS

Financial support from the National Science Foundation under Grant No. NSF MSS 9112311 and INT 8912384 is gratefully acknowledged. Deep appreciation is due to Drs. C. A. Anderson and J. Bennett at LANL for their close cooperation.

APPENDIX I. REFERENCES

Anderson, C. A., Bennett, J. G., and Dove, R. C. (1984). *Seismic category-I structures program: current status and program plan for FY84-FY85; appendix A*, Los Alamos National Laboratory, Los Alamos, N.M.

Anderson, F. E., Hanson, R. J., Murphy, H. L., Newmark, N. M., and Merit, P. W. (1964). *Design of structures to resist nuclear weapons effects*. ASCE, New York, N.Y.

Antebi, J., Utku, S., and Hansen, J. R. (1960). "The response of shear walls to dynamic loads." *Rep.*, Dept. of Civ. and Sanitary Engrg., Massachusetts Inst. of Tech. (MIT), Cambridge, Mass.

Barda, F., Hanson, J. M., and Corley, W. G. (1976). "An investigation of the design and repair of low-rise shear walls." *PCA Res. and Development Bull. RD035D*, Portland Cement Association, Skokie, Ill.

Benjamin, J. R., and Williams, H. A. (1957). "The behavior of one-story reinforced concrete shear walls." *J. Struct. Engrg. Div.*, ASCE, 83(3), 1254-1–1254-49.

Cardenas, A. E., Russell, H. G., and Corley, W. G. (1980). "Strength of low-rise structural walls." *Reinforced concrete structures subject to wind and earthquake forces*; *SP 63-10*, American Concrete Institute (ACI), Detroit, Mich., 221–224.

Cheng, F. Y. (1981). "Inelastic analysis of 3-D mixed steel and reinforced concrete seismic building systems." *J. Computers and Struct.*, 13(1-2), 189–196.

Cheng, F. Y., and Mertz, G. E. (1989). "Inelastic seismic response of reinforced concrete low-rise shear walls and building structures." *NSF Rep.*; *NTIS No. PB90-123217*, U.S. Dept. of Commerce, Washington, D.C.

Cheng, F. Y. (1993). *Matrix analysis of dynamic and seismic structures*. CE 424 Notes, Univ. of MO-Rolla, Rolla, MO.

Coladant, C., and Foure, B. (1989). "Experimental behavior of RC shear walls for NPP." *Trans., 10th Int. Conf. on Struct. Mech. in Reactor Tech., Vol. H*, AASMiRT, 245–249.

Dove, R. C., Endebrock, E. G., Dunwoody, W. E., and Bennett, J. G. (1985). "Seismic test on models of reinforced concrete category I buildings." *Proc., 8th Int. Conf. on Struct. Mech. in Reactor Tech.*, AASMiRT, Brussels, Belgium.

Galletly, G. D. (1952). "Behavior of reinforced concrete shear walls under static load." *Rep.*, Dept. of Civ. and Sanitary Engrg., Massachusetts Inst. of Tech. (MIT), Cambridge, Mass.

Gilbert, R. I., and Warner, R. F. (1978). "Tension stiffening in reinforced concrete slabs." *J. Struct. Engrg. Div.*, ASCE, 104(12), 1885–1900.

Hsu, T. C., and Mo, Y. L. (1984). "Softening of concrete in low-rise shear walls." *Res. Rep. UHCE 84-8*, Civ. Engrg. Dept., University of Houston, Houston, Tex.

Kabeyasawa, T., Shiohara, H., Otani, S., and Aoyama, H. (1983). "Analysis of the

full-scale seven-story reinforced concrete test structure." *J. Fac. of Engrg.*, Tokyo, Japan, XXXVII(2), 431–478.
Ma, S. M., Popov, E. P., and Bertero, V. V. (1976). "Experimental and analytical studies on the hysteretic behavior of reinforced concrete rectangular and T-beams." *Rep. No. EERC-76/2*, Earthquake Engrg. Res. Ctr., University of California, Berkeley, Calif.
Paulay, T., Priestley, M. J. N., and Synge, A. J. (1982). "Ductility in earthquake resisting squat shearwalls." *ACI J.*, 79(26), 257–269.
Sheu, M. S. (1988). "Behavior of low rise R.C. shear walls subjected to reversed cyclic loading." *Tech. Rep. to the National Science Council*, Arch. Engrg. Dept., National Cheng Kung University, Tainan, Taiwan.
Vallenas, J. M., Bertero, V. V., and Popov, E. P. (1979). "Hysteretic behavior of reinforced concrete structural walls." *Rep. No. EERC-79/20*, Earthquake Engrg. Res. Ctr., University of California, Berkeley, Calif.
Vecchio, F., and Collins, M. P. (1982). "The response of reinforced concrete to in-plane shear and normal stresses." *Pub. No. 82-03*, Dept. of Civ. Engrg., University of Toronto, Toronto, Canada.
Wang, F., Gantenbein, F., Delbera, J., and Duretz, C. (1989). "Seismic behavior of reinforced concrete shear walls." *Trans., 10th Int. Conf. on Struct. Mech. in Reactor Tech., Vol. K1*, AASMiRT, 473–478.
Watabe, M., Fukuzawa, R., Chiba, O., and Hatori, T. (1989). "Study on load-deflection characteristics of heavily reinforced concrete shear walls." *Trans., 10th Int. Conf. on Struct. Mech. in Reactor Tech., Vol. H.*, AASMiRT, 209–214.

APPENDIX II. NOTATION

The following symbols are used in this paper:

$[A]$ = transformation matrix;
D = displacement;
E_c = modulus of elasticity for concrete;
f_c = concrete compressive stress;
f'_c = ultimate concrete compressive stress;
f'_{cr} = concrete tensile crack stress;
e_b = excursion ratio for bending;
e_s = excursion ratio for shear;
h = height;
K = stiffness;
$[SI]$ = spring stiffness matrix;
V = shear;
γ = shear strain;
Δt = time step;
δ = deformation at gage location;
ε = strain;
θ = rotation;
μ = ductility;
σ = stress; and
ϕ = curvature.

J. Struct. Eng., 1993, 119(11): 3255-3275